Dalton Transactions

Cite this: *Dalton Trans.*, 2012, **41**, 3758

www.rsc.org/dalton

PAPER

The *para*-substituent effect and pH-dependence of the organometallic Baeyer–Villiger oxidation of rhenium–carbon bonds

Mu-Jeng Cheng,[a] Steven M. Bischof,[b] Robert J. Nielsen,*[a] William A. Goddard III,[a] T. Brent Gunnoe[c] and Roy A. Periana[b]

Received 19th October 2011, Accepted 21st December 2011
DOI: 10.1039/c2dt11984f

We studied the Baeyer–Villiger (BV) type oxidation of phenylrhenium trioxide (PTO) by H_2O_2 in the aqueous phase using Quantum Mechanics (density functional theory with the M06 functional) focusing on how the solution pH and the *para*-substituent affect the Gibbs free energy surfaces. For both PTO and MTO (methylrhenium trioxide) cases, we find that for pH > 1 the BV pathway having OH^- as the leaving group is lower in energy than the one involving simultaneous protonation of hydroxide. We also find that during this organometallic BV oxidation, the migrating phenyl is a nucleophile so that substituting functional groups in the *para*-position of phenyl with increased electron-donating character lowers the migration barrier, just as in organic BV reactions. However, this substituent effect also pushes electron density to Re, impeding HOO^- coordination and slowing down the reaction. This is in direct contrast to the organic analog, in which *para*-substitution has an insignificant influence on 1,2-addition of peracids. Due to the competition of the two opposing effects and the dependence of the resting state on pH and concentration, the reaction rate of the organometallic BV oxidation is surprisingly unaffected by *para*-substitution.

Introduction

The development of an efficient oxy-functionalization reaction that can be integrated with C–H activation reactions is a key challenge in developing selective, low-temperature (<250 °C) hydrocarbon oxidation catalysts. Facile oxy-functionalization reactions of nucleophilic $M^{\delta+}$–$R^{\delta-}$ complexes are rare,[1–5] although functionalizations are well-known for $M^{\delta-}$–$R^{\delta+}$ intermediates of more electronegative metals.[6–8]

Some of us reported recently both theory and experiments on the reaction of methylrhenium trioxide (CH_3–ReO_3, MTO) with oxidants (H_2O_2, PhIO, and IO_4^-) in the aqueous phase.[2,9] We concluded that the reaction proceeds through a Baeyer–Villiger (BV) type transition state[9] leading to formation of methanol in high yields (>80%). More recently, we studied the oxidation of 2,4,6-trimethylphenylrhenium trioxide (Mes–ReO_3, MesTO) in similar conditions.[4] We found that the lowest-barrier pathway is also through a BV type oxygen insertion, and that the replacement of alkyl by aryl migrating groups leads to an increase in the reaction rate.

To aid the understanding of how this stoichiometric transformation might be integrated into complete catalytic cycles, we utilized density functional theory (M06 functional)[10] to study the effect of *para*-substitution on the oxidation of phenylrhenium trioxide (Ph–ReO_3, PTO) by H_2O_2. We also investigated the pH-dependence of this BV type oxidation, since the rate of complementary steps such as substrate coordination, C–H cleavage, and oxidation often are pH dependent.[11–15]

Results and discussion

We began this study by calculating the aqueous phase Gibbs free energy surface of the oxidation of PTO by H_2O_2 (1 M) at pH = 7 and comparing it to that of MTO (Scheme 1). The weaker electron-donating ability of phenyl relative to methyl[16] leads to a less electron-rich Re center and stronger coordination of HOO^- to PTO. The coordination of HOO^- to Re is 0.5 kcal mol^{-1} downhill for PTO, whereas it is 3.3 kcal mol^{-1} uphill for MTO (BV–OH pathway). The barrier for oxy-insertion is 11.7 kcal mol^{-1} for PTO; whereas, it is 23.2 kcal mol^{-1} for MTO. This suggests that PTO is more reactive toward the oxidation than MTO, consistent with the instantaneous reaction of PTO upon mixing at room temperature.[4] The higher migratory aptitude of phenyl over methyl is also observed in the organic Baeyer–Villiger,[17] pinacol,[18] and Wagner–Meerwein rearrangements.[19]

This trend can be explained by an interaction of the phenyl π-orbitals with an antibonding linear combination of Re-d_π and O-p_π orbitals which helps stabilize the transition state

[a]*Materials and Process Simulation Center, California Institute of Technology, Pasadena, California 91125, USA. E-mail: smith@wag.caltech.edu*
[b]*The Scripps Energy & Materials Center, Department of Chemistry, The Scripps Research Institute, Jupiter, FL 33458, USA*
[c]*Department of Chemistry, University of Virginia, Charlottesville, Virginia 22904, USA*

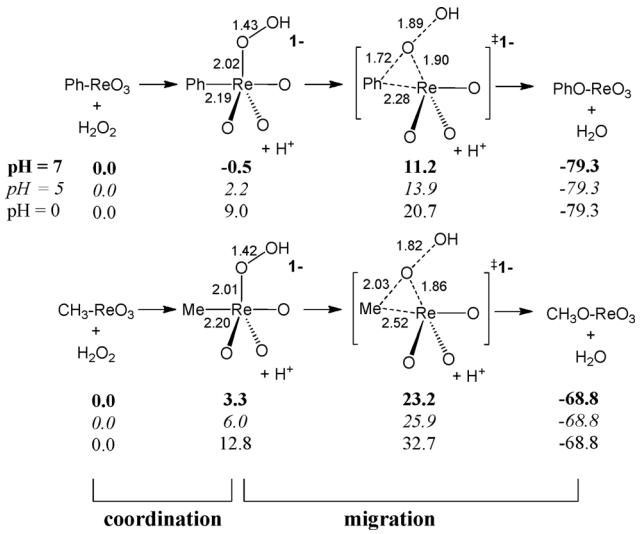

Scheme 1 Gibbs free energy (kcal mol^{-1}) surfaces of PTO and MTO Baeyer–Villiger oxidation with a hydroxide leaving group, including aqueous solvation (BV–OH-pathway).

(Scheme 2).[20,21] A similar orbital interaction is also responsible for a facile Ph 1,2-migration across the Re–O bonds of a Re(VII) bis-oxo system.[1,22] Our calculations also suggest that, similar to MTO, the oxidation of PTO by H_2O_2 is highly exergonic (ΔG = −79.9 kcal mol^{-1}) and thus irreversible, consistent with experiments.[2,4]

Interestingly, at the transition state (TS), methyl is more distant from the Re moiety ($R_{C–Re}$ = 2.52 Å, $R_{C–O}$ = 2.03 Å) than phenyl ($R_{C–Re}$ = 2.28 Å, $R_{C–O}$ = 1.72 Å). This led us to suspect that a significant amount of singlet diradical character may exist in this TS, and that the electronic structure at the TS might not be well described by the usual spin-restricted density functional formalism (R-M06). To test this we carried out a CCSD calculation[23] at the R-M06-optimized TS structure yielding a T1 diagnostic[24] of 0.027. This value is slightly higher than the 0.02 threshold suggested for determining whether single determinant methods can be successfully applied.[24] The T1 diagnostic is only 0.021 for the PTO TS.

However, full optimization of the MTO TS using CCSD leads to a structure ($R_{C–Re}$ = 2.58 Å, $R_{C–O}$ = 2.07 Å, and $R_{O–O}$ = 1.84 Å) that is almost identical to that from the R-M06 functional. Moreover, CCSD gives a barrier (electronic energy only with LACVP** basis set) of 35.0 kcal mol^{-1}, which is also similar to 31.1 kcal mol^{-1} from R-M06. Therefore, we conclude

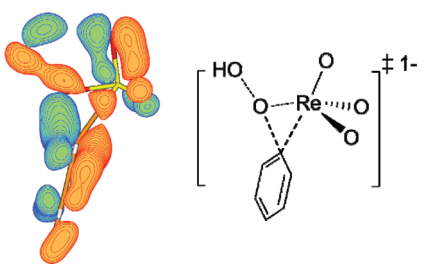

Scheme 2 Phenyl aromatic orbital overlapping the antibonding linear combination of Re-dπ and O-pπ orbitals.

although this organometallic BV transition state possesses some singlet diradical character, most of its electronic structure can be captured by R-M06.

In contrast to the facile BV type pathway, we find that the direct 1,2-phenyl migration across a Re–oxo bond poses a barrier of 43.9 kcal mol^{-1} (48.0 kcal mol^{-1} when only gas phase electronic energies from LACV3P++** basis set are considered, Scheme 3). Brown and Mayer have reported a similar, but facile, 1,2-phenyl migration in the rhenium(VII) dioxo phenyl complex ($TpReO_2Ph^+$; Tp = hydridotris(pyrazolyl)borate) with a Gibbs free energy barrier of only 20.9 kcal mol^{-1}.[1] Comparing the electronic energy of the two migration reactions, we find that the migration barrier of $TpReO_2Ph^{+1}$ is 23.3 kcal mol^{-1} lower than that of Ph–ReO_3. For $TpReO_2Ph^{+1}$, the migration leads to a stable five-coordinate product (−10.7 kcal mol^{-1} downhill compared to the reactant), whereas for Ph–ReO_3 the migration leads to the formation of an unstable three-coordinate Re complex (18.6 kcal mol^{-1} uphill). High coordination stabilizes products and destabilizes the initial Re–C bond through the orthogonalization of covalent and dative bonding orbitals. Also, the Re–oxo moiety of the Tp complex is more electrophilic, as determined either by the core orbital energies (the Re-5s and the O-1s orbitals are 1.0 eV and 1.2 eV deeper in the Tp complex, respectively) or oxo Mulliken charges (−0.55 in the Tp complex and −0.65 in PTO). These suggest that, for d^0 oxo complexes, the thermodynamics and kinetics of direct migration are promoted by a high coordination number and strong electrophilicity.

In the BV reaction, OH^- is liberated and eventually neutralized by protonation (BV–OH pathway); thus the reaction barrier may be lowered if the leaving group is H_2O instead of OH^- (BV–H_2O pathway). This new pathway has not been fully investigated before,[4,9] so we examined this possibility herein. Concurrently, we explored the influence of pH on the two different pathways. We located two types of transition states for the BV–H_2O energy surface (Scheme 4). In the top example, a proton from solvent (represented by three explicit water molecules in addition to the polarizable continuum solvent) is transferred to the OH^- to form H_2O water during the course of the migration. In the second case, the proton transfer is intramolecular: a proton bound to one of the three oxo groups (presumably provided by H_2O_2 initially) is transferred to OH^- to form H_2O. The Gibbs

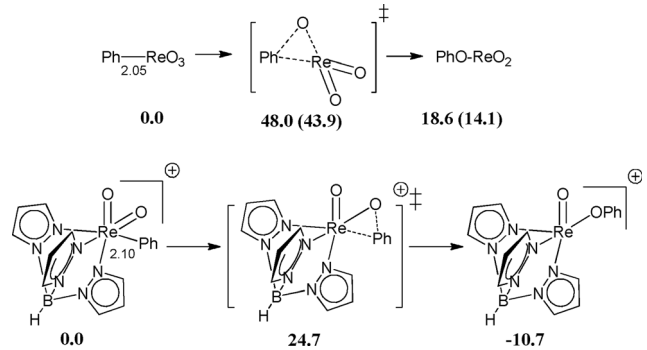

Scheme 3 Gas phase electronic energy surfaces of direct phenyl migrations across Re=O bonds (kcal mol^{-1}, Gibbs free energies including aqueous solvation in parentheses, initial Re–C bond lengths marked in Angstroms).

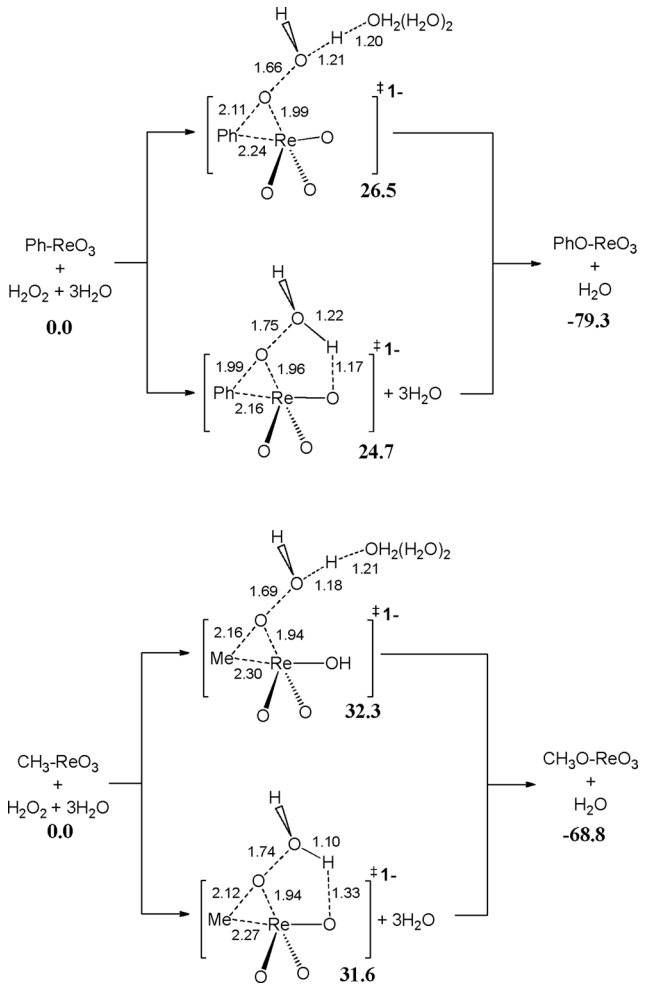

Scheme 4 Gibbs free energy surfaces of PTO and MTO Baeyer–Villiger oxidation with H_2O as leaving group including aqueous solvation (BV–H_2O pathway, unit is in kcal mol^{-1}).

free energy barriers at pH = 7 are 27.0 and 25.2 kcal mol^{-1} for PTO and 32.3 and 31.6 kcal mol^{-1} for MTO (taking the peroxide complex as resting state for R = Ph). Importantly, these barriers are much higher than those with OH^- as a leaving group (11.7 and 23.2 kcal mol^{-1} for PTO and MTO, respectively). This suggests that despite having a poorer leaving group, BV–OH is still a more favorable pathway than BV–H_2O at pH = 7.

In the BV–OH pathway one proton is released from hydrogen peroxide upon coordination to R–ReO_3 (R = CH_3, Ph). This suggests that the coordination energies and the overall BV barriers are pH-dependent. In contrast, since no proton is liberated in BV–H_2O, its overall barrier is pH independent. Accordingly, a change in solution pH may change which pathway has the lowest barrier. Since it is well known that trioxorhenium–hydrocarbyl bonds hydrolyze rapidly in basic aqueous solutions, but slowly in acidic media,[25,26] we will discuss only the low-pH regime here.

Decreasing pH disfavors liberation of a proton, and therefore destabilizes the hydrogen peroxide complex and the BV–OH transition state. The hydrocarbyl migration barrier remains unaffected, but the overall barrier increases as the pH value decreases. For example, for the PTO system where pH = 5, the coordination energy is uphill by 2.2 kcal mol^{-1} and the overall barrier is increased to 13.9 kcal mol^{-1} (Scheme 1). As the environment becomes more acidic, the overall barrier of the pathway BV–OH increases, whereas that of BV–H_2O remains unchanged. Eventually, under strongly acidic conditions, BV–H_2O becomes the most favorable low energy pathway. Our calculations suggest that for PTO, BV–H_2O would be more favorable than BV–OH only below pH = −2.8, and for MTO the crossover takes place at pH = 0.9. Since BV–OH is energetically more favorable than BV–H_2O for pH > 1, only BV–OH is considered in the following Hammett study.

Analyzing the variation of electron density in PTO during the phenyl migration step using fragment Mulliken charges, we find that significant charge variation takes place only in the hydroxide leaving group and the migrating phenyl group (Fig. 1). Along the intrinsic reaction coordinate (IRC), electron density accumulates on OH as indicated by its Mulliken charge which varies from 0.0 to −0.7 (as hydroxyl transforms to hydroxide). Charge leaves the phenyl group, as indicated by its Mulliken charge changing from −0.2 to 0.4. Thus Ph plays the role of nucleophile. This also suggests that the migration step should be accelerated when the *para*-position of Ph is substituted with a more electron-donating group.

We therefore replaced hydrogen at the *para*-position in PTO by various electron-withdrawing and electron-donating substituents (*p*-X–C_6H_4–ReO_3, X = CF_3, CH_3, OCH_3, OH, and NH_2). Indeed, we find that as X becomes more electron-donating, the migration barriers (the Gibbs free energy difference between hydrogen peroxide complexes and BV transition states) decrease from 14.4 (X = CF_3), 11.7 (H), 10.4 (CH_3), 9.8 (OCH_3), 9.6 (OH), to 8.4 (NH_2) kcal mol^{-1} (Table 1). Indeed we find a good correlation (R^2 = 0.99) between those barriers and the Hammett parameter of X (the dashed line in Fig. 2). A similar trend is also observed in the analogous organic BV reaction[27] and in a recent

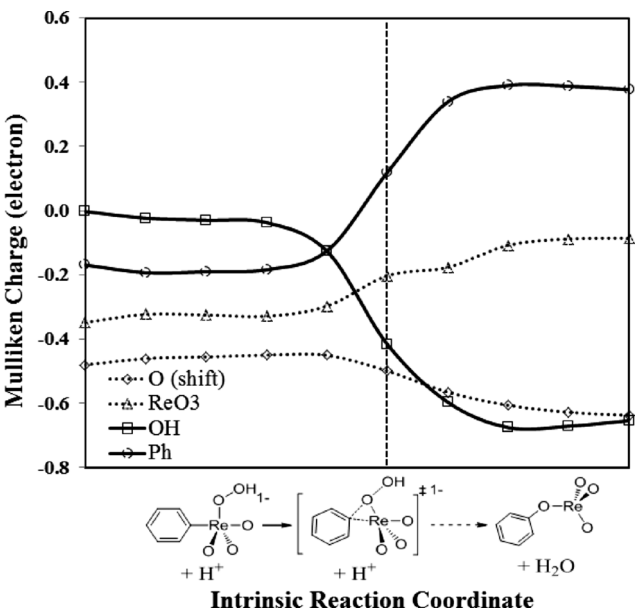

Fig. 1 Variation of the fragment Mulliken charges along the BV intrinsic reaction coordinate based on M06/LACVP** level with solvent effect (the position of TS is marked by the vertical dashed line).

Table 1 Gibbs free energy surfaces of the BV oxidation of *p*-X–C_6H_4–ReO_3 (X = CF_3, CH_3, OCH_3, OH, and NH_2) by H_2O_2 at pH = 7 including aqueous solvation (kcal mol^{-1})

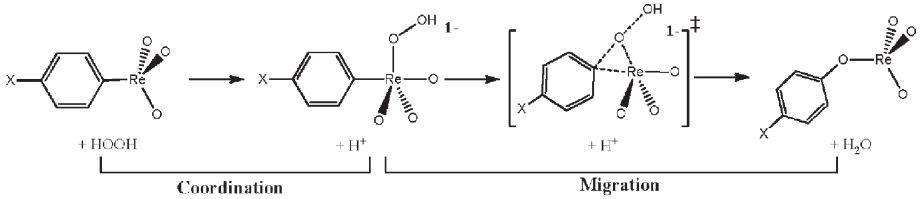

X				
CF_3	0.0	−4.3	10.1	−80.6
H	0.0	−0.5	11.2	−79.3
CH_3	0.0	1.5	11.9	−77.8
OCH_3	0.0	2.9	12.7	−73.7
OH	0.0	2.3	11.9	−75.3
NH_2	0.0	5.5	13.9	−73.5

computational study of BV insertion within Pt(II)–aryl complexes.[28]

An examination of the coordination energy shows that a more electron-donating X impedes the coordination of HOO^- to Re. The effect is large enough that the total BV barrier depends on the substituent in the opposite sense of the migration barrier. The coordination energy increases from −4.3, −0.5, 1.5, 2.9, 2.3, to 5.5 kcal mol^{-1} for X = CF_3, H, CH_3, OCH_3, OH, and NH_2, which correlate well (R^2 = 0.98) to the Hammett parameter of X (the solid line in Fig. 2). The *para*-substituent also changes the identity of the ground state (at 1 M H_2O_2): thus for X = CF_3 and H, the ground state is the hydrogen peroxide intermediate, but for X = CH_3, OCH_3, OH, and NH_2, it is the aryl rhenium trioxide.

The substituent effect leads to variations in the coordination energy (9.8 kcal mol^{-1}), which are even larger than for the migration barrier (6.0 kcal mol^{-1}). Because of compensation by two opposing influences and the change of the ground state species, the overall BV reaction barriers (13.9, 11.9, 12.7, 11.9, 11.7, and 14.4 kcal mol^{-1} for X = CF_3, H, CH_3, OCH_3, OH, and NH_2, respectively) depend erratically on the *p*-substituent on phenyl with a poor correlation between the reaction rate and the Hammett parameter of X (Fig. 3, black line).[29]

This is contrary to the results for the analogous organic BV reaction, in which the substituent effect shows a very profound influence on the reaction rate. The BV oxidation of ketones by peracids in aprotic solvents can also be partitioned into two similar steps (Scheme 5): (1) 1,2-addition of peracid to the ketone forming a tetrahedral intermediate (Criegee intermediate), and (2) the migration of a hydrocarbyl group to oxygen with simultaneous loss of a carboxylic acid. Reyes *et al.* studied the *p*-substituent effect on the oxidation of acetophenones by means of DFT.[30] They found that X substitution has a similar influence on the migration barrier as in the PTO system. However, for the 1,2-addition step, the substituent effect is insignificant. This is because a more electron-donating X, pushes electron density both to carbon (impeding the addition) and to the ketone oxo

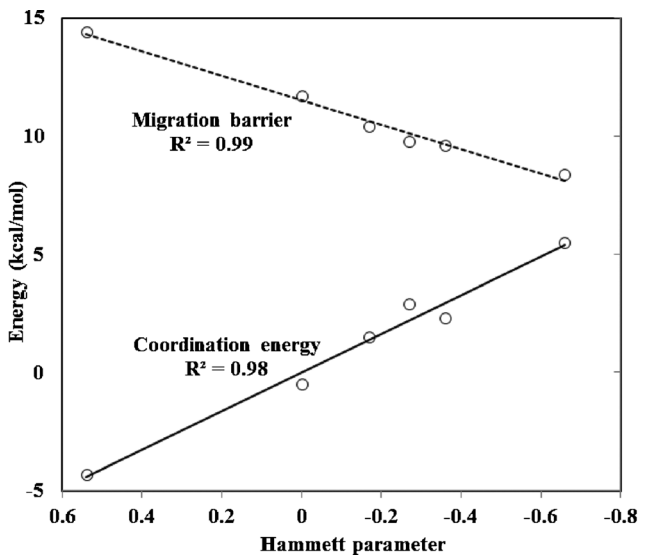

Fig. 2 Correlations between the coordination energies and phenyl migration barrier to the Hammett's parameter of X, which is 0.54, 0.0, −0.17, −0.27, −0.36, and −0.66 for CF_3, H, CH_3, OCH_3, OH, and NH_2, respectively.[16]

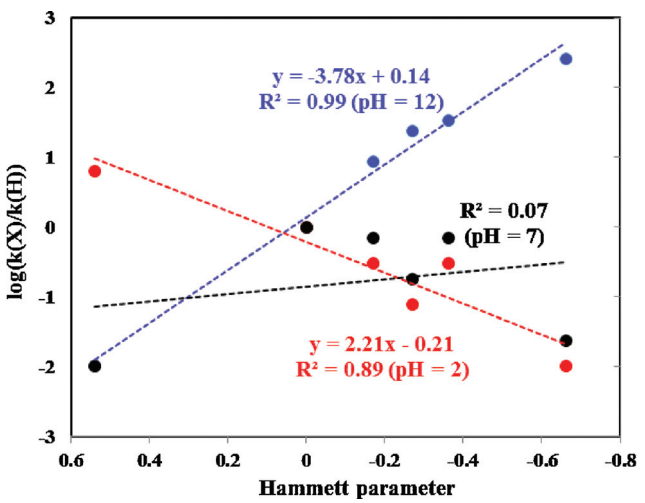

Fig. 3 Correlations between the reaction rates at different pH to the Hammett's parameter of X.

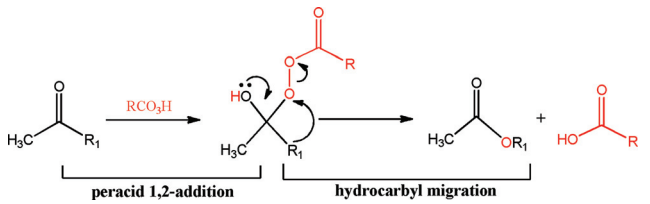

Scheme 5 Organic Baeyer–Villiger reaction of ketone with a peracid.

(increasing its basicity and therefore facilitating the addition step). The overall barrier depends only on the migration barrier, which is shown to decrease as X becomes more electron-donating.

Since changing acidity can change the coordination energy and the identity of the ground state species, the reaction rate (or overall barrier) can be tuned by solution pH value. At pH = 12 and 1 M PTO and H_2O_2, the hydrogen peroxide complexes are the ground states for all X substitutions with no penalty imposed for coordinating HOO^- to the aryl rhenium trioxide species. Thus, the overall barrier is determined only by the barrier of the migration step (our calculations show that it is more favorable to bind HOO^- than HO^- by 3.9 kcal mol^{-1}). As a result, the reaction rates are higher than those in pH = 7, and are inversely proportional to the Hammett parameters (R^2 = 0.99, blue line, Fig. 3).

On the other hand, at low pH (pH = 2) or low reactant concentration, the ground state for all X groups is the arylrhenium trioxide species, and there is a larger penalty for deprotonating H_2O_2 as compared to that at pH = 7. This leads to a larger penalty for forming the hydroperoxide intermediates. Therefore, the influence of the coordination step outweighs that of migration and dominates the overall Gibbs free energy surface. As a result, the reaction rates are smaller than those at pH = 7 and are proportional to the Hammett parameter of X, showing that the reaction is decelerated when X becomes more electron-donating (red line, Fig. 3).

Conclusions

In summary, we studied the BV-type oxidation of phenyl trioxorhenium by H_2O_2 in the aqueous phase. Our coupled-cluster calculations show that although the BV-type transition state contains some singlet diradical character (especially in the MTO case), its electronic structure is still well described by R-M06. We have investigated an alternate BV pathway in which H_2O instead of OH^- is the leaving group, and find that in the pH range of interest (pH > 1), the BV pathway with OH^- as the leaving group is lower in energy than one featuring simultaneous protonation of hydroxide for both PTO and MTO cases. Based on the fragment Mulliken charges, the organometallic BV oxidation occurs with the migrating phenyl acting as a nucleophile. Accordingly, substituting an electron-donating functional group in the *para*-position of phenyl lowers the migration barrier, similar to the organic analog. However, this substituent effect also pushes electron density to Re, impeding HOO^- coordination and slowing down the reaction. This is in contrast to the organic BV oxidation, in which *para*-substitution insignificantly influences the 1,2-addition of peracids. Due to the competition of the two opposing effects and the dependence of the resting state on pH and concentration, the reaction rate of this organometallic BV oxidation does not correlate linearly on the Hammett parameters of the substituents.

The organometallic Baeyer–Villiger reaction poses a remarkably low barrier to the insertion of oxygen into metal–carbon bonds (*e.g.*, the calculated barrier for oxidizing Ph–ReO_3 to PhO–ReO_3 is only 11.7 kcal mol^{-1}). However, the disadvantage of this reaction is that if the substrate "M–R" has non-zero d-electrons, the oxidant may oxidize the metal rather than the metal–carbon bond; therefore, this reaction is not suitable for metal complexes with high-energy d-electrons. In two classes of M–R complexes this mechanism may play an important role. The first class is early transition metal complexes that have no d-electrons. However it is unlikely that species capable of activating C–H bonds can be catalytically regenerated after oxidation of those oxophilic metals. The second class is later transition metal complexes with very stable d-electrons. For example, the insertion of oxygen into palladium–aryl and nickel–aryl bonds is already known.[31–33] This class is more promising for integrating the OM-BV oxy-functionalization with alkane C–H activation, since late transition metals are known for activating alkane C–H bonds in oxidizing conditions.[11,34,35] Therefore, we will focus on those systems in the future.

Computational details

The geometry optimizations and zero-point vibrational energy (ZPVE) were carried out using the M06 functional[36,37] with the 6-31G**basis set[38,39] for all atoms except Re. For Re the first four shells of core electrons were described by the Los Alamos angular momentum projected effective core potential (ECP) using the double-ζ contraction of valence functions[40] (denoted as LACVP**).

Solvation energies were calculated using the Poisson–Boltzmann self-consistent polarizable continuum method[41,42] implemented in Jaguar[43] to represent water (dielectric constant = 80.37 and effective radius = 1.4 Å). The solvation calculations used the M06/LACVP** level of theory and the gas-phase optimized structures.

Singlet-point energy calculations were performed using the M06 functional with a larger basis set: here Re was described with the triple-ζ contraction of valence functions augmented with two f functions[44] and the core electrons were described by the same ECP; the other atoms were described with the 6-311++G** basis set.[45–47]

Unless otherwise noted, all energies discussed in this work are free energies, calculated as

$$G_{298K} = E_{elec} + G_{solv} + ZPVE + \sum_{\nu} \frac{h\nu}{e^{h\nu/kT} - 1} + \frac{n}{2}kT - T(S_{vib} + S_{rot} + S_{trans}),$$

where n = 12 accounts for the potential and kinetic energies of the translational and rotational modes and T = 298 K. The values of (S_{rot} + S_{trans}) for each Re intermediate were assumed to cancel.

The free energy of H_2O_2(aq), HOO^-(aq), and H^+(aq) at pH = 7 were calculated by adding the computed ideal gas phase Gibbs

free energy and the experimentally measured solvation free energy $\Delta G(1\ \text{atm}\rightarrow 1\ \text{M})$[48,49] and correcting for concentration *via* $G = G^\circ + kT\ln(C/C^\circ)$.

Acknowledgements

This work was fully supported by the Center for Catalytic Hydrocarbon Functionalization, an Energy Frontier Research Center, DOE DE-SC0001298.

Notes and references

1 S. N. Brown and J. M. Mayer, *J. Am. Chem. Soc.*, 1996, **118**, 12119–12133.
2 B. L. Conley, S. K. Ganesh, J. M. Gonzales, W. J. Tenn, K. J. H. Young, J. Oxgaard, W. A. Goddard and R. A. Periana, *J. Am. Chem. Soc.*, 2006, **128**, 9018–9019.
3 B. L. Conley, S. K. Ganesh, J. M. Gonzales, D. H. Ess, R. J. Nielsen, V. R. Ziatdinov, J. Oxgaard, W. A. Goddard and R. A. Periana, *Angew. Chem., Int. Ed.*, 2008, **47**, 7849–7852.
4 S. M. Bischof, M. J. Cheng, R. J. Nielsen, T. B. Gunnoe, W. A. Goddard and R. A. Periana, *Organometallics*, 2011, **30**, 2079–2082.
5 W. T. Reichle and W. L. Carrick, *J. Organomet. Chem.*, 1970, **24**, 419.
6 R. A. Periana, G. Bhalla, W. J. Tenn, K. J. H. Young, X. Y. Liu, O. Mironov, C. J. Jones and V. R. Ziatdinov, *J. Mol. Catal. A: Chem.*, 2004, **220**, 7–25.
7 M. Lersch and M. Tilset, *Chem. Rev.*, 2005, **105**, 2471–2526.
8 J. F. Hartwig, *Acc. Chem. Res.*, 1998, **31**, 852–860.
9 J. M. Gonzales, R. Distasio, R. A. Periana, W. A. Goddard and J. Oxgaard, *J. Am. Chem. Soc.*, 2007, **129**, 15794–15804.
10 All energies discussed here are Gibbs free energies from M06/LACV3P++**//LACVP** level of theory.
11 R. A. Periana, D. J. Taube, S. Gamble, H. Taube, T. Satoh and H. Fujii, *Science*, 1998, **280**, 560–564.
12 C. J. Jones, D. Taube, V. R. Ziatdinov, R. A. Periana, R. J. Nielsen, J. Oxgaard and W. A. Goddard, *Angew. Chem., Int. Ed.*, 2004, **43**, 4626–4629.
13 B. G. Hashiguchi, K. J. H. Young, M. Yousufuddin, W. A. Goddard and R. A. Periana, *J. Am. Chem. Soc.*, 2010, **132**, 12542–12545.
14 A. Hofmann, D. Jaganyi, O. Q. Munro, G. Liehr and R. van Eldik, *Inorg. Chem.*, 2003, **42**, 1688–1700.
15 M. Ahlquist, R. A. Periana and W. A. Goddard, *Chem. Commun.*, 2009, 2373–2375.
16 C. Hansch, A. Leo and R. W. Taft, *Chem. Rev.*, 1991, **91**, 165–195.
17 M. F. Hawthorne, W. D. Emmons and K. S. Mccallum, *J. Am. Chem. Soc.*, 1958, **80**, 6393–6398.
18 M. Stiles and R. P. Mayer, *J. Am. Chem. Soc.*, 1959, **81**, 1497–1503.
19 H. C. Brown and C. J. Kim, *J. Am. Chem. Soc.*, 1968, **90**, 2082.
20 K. Nakamura and Y. Osamura, *J. Am. Chem. Soc.*, 1993, **115**, 9112–9120.
21 K. Nakamura and Y. Osamura, *Tetrahedron Lett.*, 1990, **31**, 251–254.
22 M. J. Cheng, R. J. Nielsen, M. Ahlquist and W. A. Goddard, *Organometallics*, 2010, **29**, 2026–2033.
23 CCSD/LACVP** calculations are performed by Gamess package.
24 T. J. Lee and P. R. Taylor, *Int. J. Quantum. Chem.*, 1989, 199–207.
25 G. Laurenczy, F. Lukacs, R. Roulet, W. A. Herrmann and R. W. Fischer, *Organometallics*, 1996, **15**, 848–851.
26 M. M. Abu-Omar, P. J. Hansen and J. H. Espenson, *J. Am. Chem. Soc.*, 1996, **118**, 4966–4974.
27 S. L. Friess and A. H. Soloway, *J. Am. Chem. Soc.*, 1951, **73**, 3968–3972.
28 T. M. Figg, T. R. Cundari and T. B. Gunnoe, *Organometallics*, 2011, **30**, 3779–3785.
29 Efforts to prepare the functionalized Re–aryl analogs for an experimental Hammett study have not yet been successful.
30 L. Reyes, J. R. Alvarez-Idaboy and N. Mora-Diez, *J. Phys. Org. Chem.*, 2009, **22**, 643–649.
31 D. Bandyopadhyay and K. Kamaraj, *Organometallics*, 1999, **18**, 438–446.
32 P. L. Alsters, H. T. Teunissen, J. Boersma, A. L. Spek and G. Vankoten, *Organometallics*, 1993, **12**, 4691–4696.
33 K. M. Koo, G. L. Hillhouse and A. L. Rheingold, *Organometallics*, 1995, **14**, 456–460.
34 A. E. Shilov and G. B. Shul'pin, *Chem. Rev.*, 1997, **97**, 2879–2932.
35 S. S. Stahl, J. A. Labinger and J. E. Bercaw, *Angew. Chem., Int. Ed.*, 1998, **37**, 2180–2192.
36 Y. Zhao and D. G. Truhlar, *Acc. Chem. Res.*, 2008, **41**, 157–167.
37 Y. Zhao and D. G. Truhlar, *Theor. Chem. Acc.*, 2008, **120**, 215–241.
38 W. J. Hehre, R. Ditchfie and J. A. Pople, *J. Chem. Phys.*, 1972, **56**, 2257–2261.
39 M. M. Francl, W. J. Pietro, W. J. Hehre, J. S. Binkley, M. S. Gordon, D. J. Defrees and J. A. Pople, *J. Chem. Phys.*, 1982, **77**, 3654–3665.
40 P. J. Hay and W. R. Wadt, *J. Chem. Phys.*, 1985, **82**, 299–310.
41 D. J. Tannor, B. Marten, R. Murphy, R. A. Friesner, D. Sitkoff, A. Nicholls, M. Ringnalda, W. A. Goddard and B. Honig, *J. Am. Chem. Soc.*, 1994, **116**, 11875–11882.
42 B. Marten, K. Kim, C. Cortis, R. A. Friesner, R. B. Murphy, M. N. Ringnalda, D. Sitkoff and B. Honig, *J. Phys. Chem.*, 1996, **100**, 11775–11788.
43 I. P. *Jaguar 7.6*, Schrodinger, OR, 2009.
44 J. M. L. Martin and A. Sundermann, *J. Chem. Phys.*, 2001, **114**, 3408–3420.
45 A. D. Mclean and G. S. Chandler, *J. Chem. Phys.*, 1980, **72**, 5639–5648.
46 T. Clark, J. Chandrasekhar, G. W. Spitznagel and P. V. Schleyer, *J. Comput. Chem.*, 1983, **4**, 294–301.
47 M. J. Frisch, J. A. Pople and J. S. Binkley, *J. Chem. Phys.*, 1984, **80**, 3265–3269.
48 M. D. Tissandier, K. A. Cowen, W. Y. Feng, E. Gundlach, M. H. Cohen, A. D. Earhart, T. R. Tuttle and J. V. Coe, *J. Phys. Chem. A*, 1998, **102**, 9308–9308.
49 D. D. Wagman, W. H. Evans, V. B. Parker, R. H. Schumm, I. Halow, S. M. Bailey, K. L. Churney and R. L. Nuttall, *J. Phys. Chem. Ref. Data*, 1982, **11**, 1–392.